

**EVALUATION OF THE MECHANISMS FOR
INDUCING LEADING EDGE VORTEX USING
ANSYS FLUENT**

by


MOHAMED NIZAM BIN MOHAMED IDRIS

**Thesis submitted in fulfilment of the
requirements for the degree of
Bachelor of Engineering (Honours) (Aerospace Engineering)**

June 2021

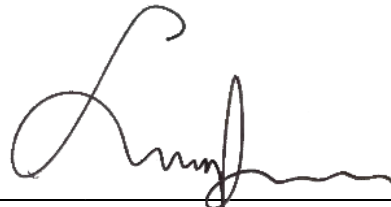
ENDORSEMENT

I, Mohamed Nizam bin Mohamed Idris hereby declare that all corrections and comments made by the supervisor and examiner have been taken consideration and rectified accordingly.



(Signature of Student)

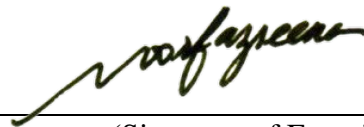
Date: 9/7/2021



(Signature of Supervisor)

Name: Dr. Norizham Bin Abdul Razak

Date:



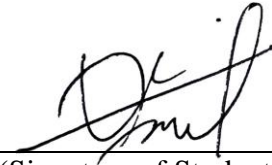
(Signature of Examiner)

Name: Dr. Noorfazreena Mohammad
Kamaruddin

Date: 9 July 2021

DECLARATION

This thesis is the result of my own investigation, except where otherwise stated and has not previously been accepted in substance for any degree and is not being concurrently submitted in candidature for any other degree



(Signature of Student)

Date: 20/6/2021

ACKNOWLEDGEMENTS

First and foremost, I would like to express my deepest and sincere gratitude to my supervisor, Dr. Norizham Bin Abdul Razak, lecturer of School of Aerospace Engineering at Universiti Sains Malaysia, for his guidance, patience, and full support throughout the completion of this study possible.

I would like to acknowledge the support from School of Aerospace Engineering, Universiti Sains Malaysia for providing the necessary facilities which had been directly used for the simulations that presented in this study. I would like to express my appreciation to CATIA Lab technical staffs for resolving technical problems and issues that I had encountered during the research.

I would also like to thank each of my coursemates and friends who have been giving me suggestions, advice, and supports in assisting me to complete this study.

Last but not least, I would like to express my gratitude to my family especially my parents, who have always provided me with unfailing support and continuous encouragement throughout my years of study.

Thank you.

EVALUATION OF THE MECHANISMS FOR INDUCING LEADING EDGE VORTEX USING ANSYS FLUENT

ABSTRACT

This thesis evaluates the mechanism for inducing leading edge vortex using synthetic jet utilising ansys fluent on an airfoil due to aerodynamic in the transitional Reynolds number regime. Two-dimensional simulations based on the concept of fluid-structure interaction at low-to-moderate Reynold's number ($6.77 \times 10^4 \leq Re \leq 6.77 \times 10^5$) are carried out on a NACA 4412 airfoil with several angles of attack using Ansys Fluent. The model of simulation that being used is the laminar flow around the airfoil. To compute the flow response of the jet synthetic from the airfoil, a graph of velocity was constructed through the simulation process to ensure that the flow on top of the jet synthetic is precise. The process of releasing the air periodically through the pore/orifice was created by adding data files through the transient table file. The simulation was simulated at different airspeeds ranging from 1 m/s to 10 m/s. The fluctuation of lift and drag coefficient was increase as the jet velocity is increase. The angle of attack of the airfoil also holds a huge role on the fluctuation effects of lift and drag coefficient. The point of separation of flow on the surface of the airfoil is found to be affected by then angle of attack and jet output speed. The wake of the airfoil at the trailing edge also can be observed to be affected by the jet output is eject through the orifice. As a result form this study, 10 m/s jet could enhance the lift and drag coefficient, but it has a major drawback. So, the optimised solution with the most enhance aerodynamic properties and minimised drawback is to use jet 10 m/s at 6° .

ABSTRAK

Tesis ini menilai mekanisme untuk mendorong pusaran tepi/hujung menggunakan jet sintetik melalui simulasi Ansys pada kerajang udara aerodinamik dalam rejim bilangan peralihan Reynolds. Simulasi dua dimensi berdasarkan konsep interaksi struktur-bendalir pada bilangan number Reynold yang rendah sehingga sederhana ($6.77 \times 10^4 \leq Re \leq 6.77 \times 10^5$) dilakukan pada kerajang udara NACA 4412 dengan beberapa sudut serangan menggunakan Ansys Fluent. Model simulasi yang digunakan adalah aliran laminar di sekitar bahagian udara. Bagi mengira tindak balas aliran sintetik jet dari kerajang udara, graf kelajuan dibina melalui proses simulasi untuk memastikan bahawa aliran di atas jet sintetik tepat ketika proses simulasi dijalankan. Proses pembebasan udara secara berkala melalui liang/lubang dibuat dengan menambahkan fail data melalui fail-jadual-sementara. Simulasi dijalankan pada kelajuan udara yang berbeza antara 1 m/s hingga 10 m/s. Fluktuasi pekali naik dan seret didapati meningkat ketika kecepatan jet meningkat. Sudut serangan udara juga berperanan besar terhadap kesan turun naik pekali daya naik dan seret. Titik pemisahan aliran pada permukaan udara didapati dipengaruhi oleh sudut serangan dan kelajuan jet. Kebangkitan udara berhalaju rendah di bahagian belakang kerajang udara juga dapat dilihat ketika keluaran jet dikeluarkan melalui lubang. Sebagai hasil kajian ini, jet 10 m/s dapat meningkatkan pekali angkat dan seret, tetapi ia mempunyai kelemahan besar sebagai kesan dari tujuhan angin. Akhir kata, penyelesaian yang dioptimumkan dengan sifat aerodinamik yang paling cekap dan kelemahan paling minimum adalah menggunakan jet 10 m/s pada sudut 6° .

TABLE OF CONTENTS

	Page
ENDORSEMENT	i
DECLARATION	ii
ACKNOWLEDGEMENTS	iii
ABSTRACT	iv
ABSTRAK	v
TABLE OF CONTENTS	vi
LIST OF FIGURES	ix
LIST OF TABLES	xiv
LIST OF ABBREVIATIONS	xv
LIST OF SYMBOLS	xvi
CHAPTER 1	1
1.1 Jet Synthetic	1
1.2 Flow Behaviour	2
1.3 Boundary Layer	3
1.4 Reynolds Number	4
1.5 Computational Fluid Dynamics (CFD)	4
1.6 Motivation	5
1.7 Objectives	6
1.8 Thesis Outline	6
CHAPTER 2	7
2.1 Flow Control	7
2.2 Passive Flow Control (PFC)	9
2.2.1 Leading Edge Slats	9
2.2.2 Vortex Generators	10
2.2.3 Airfoils with Cavity	11
2.2.4 Flow Vanes	12
2.2.5 Roughness Material	13
2.3 Active Flow Control (AFC)	17
2.3.1 Fluidic Actuators	18
2.3.2 Moving Surface/Object	20
2.4 Summary	22
CHAPTER 3	23

3.1	Parameter Setup	23
3.2	Fluid Solver	24
3.2.1	Mesh and Boundary Conditions	24
3.2.2	Setup	26
3.3	Test and Validations	29
3.3.1	Grid Independence Test	30
3.3.2	Steady Flow Validation	31
CHAPTER 4		33
4.1	Angle of Attack 0°	33
4.1.1	Lift and Drag Coefficient	33
4.1.2	Pressure Coefficient and Pressure Contour	35
4.1.3	Velocity contour	37
4.2	Angle of Attack 2°	40
4.2.1	Lift and Drag Coefficient	40
4.2.2	Pressure Coefficient and Pressure Contour	41
4.2.3	Velocity contour	46
4.3	Angle of Attack 4°	48
4.3.1	Lift and Drag Coefficient	48
4.3.2	Pressure Coefficient and Pressure Contour	49
4.3.3	Velocity contour	54
4.4	Angle of Attack 6°	56
4.4.1	Lift and Drag Coefficient	56
4.4.2	Pressure Coefficient and Pressure Contour	57
4.4.3	Velocity contour	62
4.5	Angle of Attack 8°	64
4.5.1	Lift and Drag Coefficient	64
4.5.2	Pressure Coefficient and Pressure Contour	66
4.5.3	Velocity contour	70
4.6	Angle of Attack 10°	73
4.6.1	Lift and Drag Coefficient	73
4.6.2	Pressure Coefficient and Pressure Contour	74
4.6.3	Velocity contour	79
4.7	Optimised Parameter	81
CHAPTER 5		83
5.1	Conclusions	83

5.2 Recommendations for Future Research	84
REFERENCES	85
APPENDICES	90

LIST OF FIGURES

	Page
Figure 2.1: Schematic of laminar separation bubble (Crivellini et al., 2014)	8
Figure 2.2: Configuration of leading-edge slat (Serdar Genç et al., 2020b).	10
Figure 2.3: A sketch of vortex generators installed on the surface of a wing (Serdar Genç et al., 2020a).	11
Figure 2.4: The vorticity contour plot over cavitied airfoil (Olsman & Colonius, 2010).	12
Figure 2.5: Flow vane sketch on the main body (Pechlivanoglou, 2013).	13
Figure 2.6: Sketch representation of the roughened airfoil at the leading edge (Serdar Genç et al., 2020a).	14
Figure 2.7: The comparison results of two different experiments at Reynolds number of 5×10^4 and $\alpha = 8^\circ$: (a) $k/c = 0$ (uncontrolled airfoil) and (b) $k/c = 0.003$ (Serdar GENÇ et al., 2019).	15
Figure 2.8: The combined result from numerical and smoke-wire result for the roughened airfoil (Serdar GENÇ et al., 2019).	16
Figure 2.9: Force measurement results at $k/c = 0.006$: (a) $Re = 7.5 \times 10^4$ and (b) $Re = 1 \times 10^5$ (Serdar Genc et al., 2019).	17
Figure 2.10: Schematic of a rotary valve (McManus & Magill, 1996).	19
Figure 2.11: The schematic drawing of the combustion actuators device.	20
Figure 2.12: Configuration of wind turbine blade section with active external trailing-edge flap: (a) side view; (b) bottom view; (c) layout of actuator (Sun et al., 2017).	21
Figure 2.13: Three-dimensional view of NACA 0012 with dimples (Haque, 2017.)	22
Figure 3.1: Mesh around the airfoil	25
Figure 3.2: Dimensions and boundary conditions of the computational domain.	25
Figure 3.3: The solution methods setup.	26

Figure 3.4:	The transient table format for 10 m/s.	27
Figure 3.5:	The calculation setup for the simulation.	28
Figure 3.6:	Simulation flowchart	29
Figure 3.7:	Lift coefficient plot for steady flow.	32
Figure 3.8:	Drag coefficient plot for steady flow.	32
Figure 4.1:	The lift coefficient at 0° (aoa) for every timesteps and jet velocity.	34
Figure 4.2:	The drag coefficient at 0° (aoa) for every timesteps and jet velocity.....	34
Figure 4.3:	The pressure contour at t=4 s, 1 m/s of jet velocity.....	35
Figure 4.4:	The pressure contour at t=5 s, 1 m/s of jet velocity.....	36
Figure 4.5:	The pressure contour at t=4 s, 10 m/s of jet velocity.....	36
Figure 4.6:	The pressure contour at t=5 s, 10 m/s of jet velocity.....	37
Figure 4.7:	The velocity contour at t=4 s, 1 m/s of jet velocity.	38
Figure 4.8:	The velocity contour at t=5 s, 1 m/s of jet velocity.	38
Figure 4.9:	The velocity contour at t=4 s, 10 m/s of jet velocity.	39
Figure 4.10:	The velocity contour at t=5 s, 10 m/s of jet velocity.	39
Figure 4.11:	The lift coefficient at 2° (aoa) for every timesteps and jet velocity.	40
Figure 4.12:	The drag coefficient at 2° (aoa) for every timesteps and jet velocity.....	40
Figure 4.13:	The pressure coefficient at t=4 s, 1 m/s of jet velocity.....	42
Figure 4.14:	The pressure contour at t=4 s, 1 m/s of jet velocity.....	42
Figure 4.15:	The pressure coefficient at t=5 s, 1 m/s of jet velocity.....	43
Figure 4.16:	The pressure contour at t=5 s, 1 m/s of jet velocity.....	43
Figure 4.17:	The pressure coefficient at t=4 s, 10 m/s of jet velocity.....	44
Figure 4.18:	The pressure contour at t=4 s, 10 m/s of jet velocity.....	44
Figure 4.19:	The pressure coefficient at t=5 s, 10 m/s of jet velocity.....	45
Figure 4.20:	The pressure contour at t=5 s, 10 m/s of jet velocity.....	45

Figure 4.21: The velocity contour at t=4 s, 1 m/s of jet velocity.....	46
Figure 4. 22: The velocity contour at t=5 s, 1 m/s of jet velocity.....	46
Figure 4.23: The velocity contour at t=4 s, 10 m/s of jet velocity.....	47
Figure 4.24: The velocity contour at t=5 s, 10 m/s of jet velocity.....	47
Figure 4.25: The lift coefficient at 4° (aoa) for every timesteps and jet velocity	48
Figure 4.26: The drag coefficient at 4° (aoa) for every timesteps and jet velocity	48
Figure 4.27: The pressure coefficient at t=7 s, 1 m/s of jet velocity.....	50
Figure 4.28: The pressure contour at t=7 s, 1 m/s of jet velocity.....	50
Figure 4.29: The pressure coefficient at t=8.5 s, 1 m/s of jet velocity.....	51
Figure 4.30: The pressure contour at t=8.5 s, 1 m/s of jet velocity.....	51
Figure 4.31: The pressure coefficient at t=7 s, 10 m/s of jet velocity.....	52
Figure 4.32: The pressure contour at t=7 s, 10 m/s of jet velocity.....	52
Figure 4.33: The pressure coefficient at t=8.5 s, 10 m/s of jet velocity.....	53
Figure 4.34: The pressure contour at t=8.5 s, 10 m/s of jet velocity.....	53
Figure 4.35: The velocity contour at t=7 s, 1 m/s of jet velocity.....	54
Figure 4.36: The velocity contour at t=8.5 s, 1 m/s of jet velocity.....	54
Figure 4.37: The velocity contour at t=7 s, 10 m/s of jet velocity.....	55
Figure 4.38: The velocity contour at t=5 s, 10 m/s of jet velocity.....	55
Figure 4.39: The lift coefficient at 6° (aoa) for every timesteps and jet velocity	56
Figure 4.40: The drag coefficient at 6° (aoa) for every timesteps and jet velocity.....	56
Figure 4.41: The pressure coefficient at t=5 s, 2 m/s of jet velocity.....	58
Figure 4.42: The pressure contour at t=5 s, 2 m/s of jet velocity.....	58
Figure 4.43: The pressure coefficient at t=6.5 s, 2 m/s of jet velocity.....	59
Figure 4.44: The pressure contour at t=6.5s, 2 m/s of jet velocity.....	59
Figure 4.45: The pressure coefficient at t=5 s, 10 m/s of jet velocity.....	60

Figure 4.46: The pressure contour at t=5 s, 10 m/s of jet velocity.....	60
Figure 4.47: The pressure coefficient at t=6.5 s, 10 m/s of jet velocity.....	61
Figure 4.48: The pressure contour at t=6.5 s, 10 m/s of jet velocity.....	61
Figure 4.49: The velocity contour at t=5 s, 2 m/s of jet velocity.....	62
Figure 4.50: The velocity contour at t=6.5 s, 2 m/s of jet velocity.....	62
Figure 4.51: The velocity contour at t=5 s, 10 m/s of jet velocity.....	63
Figure 4.52: The velocity contour at t=6.5 s, 10 m/s of jet velocity.....	63
Figure 4.53: The lift coefficient at 8° (aoa) for every timesteps and jet velocity	64
Figure 4.54: The drag coefficient at 8° (aoa) for every timesteps and jet velocity.....	65
Figure 4.55: The pressure coefficient at t=5 s, 1 m/s of jet velocity.....	66
Figure 4.56: The pressure contour at t=5 s, 1 m/s of jet velocity.....	67
Figure 4.57: The pressure coefficient at t=6.5 s, 1 m/s of jet velocity.....	67
Figure 4.58: The pressure contour at t=6.5s, 1 m/s of jet velocity.....	67
Figure 4.59: The pressure coefficient at t=5 s, 10 m/s of jet velocity.....	68
Figure 4.60: The pressure contour at t=5 s, 10 m/s of jet velocity.....	68
Figure 4.61: The pressure coefficient at t=6.5 s, 10 m/s of jet velocity.....	69
Figure 4.62: The pressure contour at t=6.5 s, 10 m/s of jet velocity.....	69
Figure 4.63: The velocity contour at t=5 s, 1 m/s of jet velocity.....	70
Figure 4.64: The velocity contour at t=6.5 s, 2 m/s of jet velocity.....	71
Figure 4.65: The velocity contour at t=6.55 s, 10 m/s of jet velocity.....	71
Figure 4.66: The velocity contour at t=6.5 s, 10 m/s of jet velocity.....	72
Figure 4.67: The lift coefficient at 10° (aoa) for every timesteps and jet velocity	73
Figure 4.68: The drag coefficient at 10° (aoa) for every timesteps and jet velocity.....	73
Figure 4.69: The pressure coefficient at t=5 s, 1 m/s of jet velocity.....	75
Figure 4.70: The pressure contour at t=5 s, 1 m/s of jet velocity.....	75

Figure 4.71: The pressure coefficient at t=6.5 s, 1 m/s of jet velocity.....	76
Figure 4.72: The pressure contour at t=6.5s, 1 m/s of jet velocity.....	76
Figure 4.73: The pressure coefficient at t=5 s, 10 m/s of jet velocity.....	77
Figure 4.74: The pressure contour at t=5 s, 10 m/s of jet velocity.....	77
Figure 4.75: The pressure coefficient at t=6.5 s, 10 m/s of jet velocity.....	78
Figure 4.76: The pressure contour at t=6.5 s, 10 m/s of jet velocity.....	78
Figure 4.77: The velocity contour at t=5 s, 1 m/s of jet velocity.	79
Figure 4.78: The velocity contour at t=6.5 s, 2 m/s of jet velocity.	80
Figure 4.79: The velocity contour at t=6.55 s, 10 m/s of jet velocity.	80
Figure 4.80: The velocity contour at t=6.5 s, 10 m/s of jet velocity.	81
Figure 4.81: The lift-to-drag ratio of 10 m/s jet velocity for every fluctuation timesteps.	82

LIST OF TABLES

	Page
Table 3.1: Properties of air and airfoil.	23
Table 3.2: Grid independence test result.	30

LIST OF ABBREVIATIONS

AFC	Active Flow Control
AOA	Angle of Attack
CFD	Computational Fluid Dynamics
DNS	Direct Numerical Simulation
DOF	Degree of Freedom
FSI	Fluid-Structure Interaction
LES	Large Eddy Simulation
LEV	Leading Edge Vortex
LSB	Laminar Separation Bubble
NACA	National Advisory Committee for Aeronautics
PISO	Pressure-Implicit with Splitting of Operators
RANS	Reynolds-Averaged Navier-Stokes
UDF	User-Defined Function

LIST OF SYMBOLS

ρ	fluid density	kg/m ³
Re	Reynolds number	–
l_c	characteristic length	m
Δt	time step size	s
V	free stream airspeed	m/s
b	airfoil semi-chord length	m
c	airfoil chord length	m
l	lift per unit span	N/m
α	angle of attack	deg or rad
μ	dynamic viscosity	kgm ⁻¹ s ⁻¹

CHAPTER 1

INTRODUCTION

1.1 Jet Synthetic

Drag reduction and increase in lift have been considered as an influence to enhance the overall performance of aircraft. These factors could boost the fuel consumption, stability, endurance and maneuverability of airplanes. Research shown that flow control has a great impact on the performance of an aircraft, there are two types of flow separation control, the active and the passive flow control. Active Flow Control (AFC), is mainly addition of momentum at precise locations of the boundary layer, is one of the methods that have a great potential to do so.

Active flow control been classified into the following solutions (Cattafesta & Sheplak, 2011): 1- moving body actuators that have the aim to induce local fluid motion without the addition of mass. 2- plasma actuators that have been studied recently due to the fast time response and finally 3- fluidic actuators which are most common type of actuators, and their main function is to inject/suck fluid from/to the boundary layer.

Jet synthetic is the actuators in the fluidic actuators that have zero-net-mass-flux. This show that jet synthetic has good feasibility for industrial applications and have a huge impact on controlling flow separation (Glezer & Amitay, 2002)(Gritskevich et al., 2012) (Findanis & Ahmed, 2008). To control flow separation is based on the ability to stabilize the boundary layer by adding/removing momentum to/from the boundary layer, this includes the formation of vortical structures. This factor in return will promote boundary layer mixing and exchange the momentum outer and inner parts of the boundary layer.

For the past few decades, these jets synthetic have been implemented in numerous airfoils and by using various numerical models. Researchers have used the Reynolds-averaged Navier Stokes (RANS) equations to compute the flow around a NACA0012 airfoil using a synthetic jet (Donovan et al., 1998). A significant increase in lift (29%) was observed in the post-stall regime. Donovan prove that the jet velocity is one of the main variables that is very essential to define the momentum coefficient.

Recently, (McCormick, 2000) also investigated steady-blowing jet of high jet momentum in both simulation and wind tunnel tests. Their experiments concluded that that the steady-blowing jet which is normal to the airfoil chord is able to suppress the moment stall that occurs on an airfoil however, this process comes at a bad output of non-negligible reduction in the aerodynamic lift throughout the process. The main aim of the work is to increase the airfoil efficiency, at different angles of attack and different jet velocities.

1.2 Flow Behaviour

Flow characteristic on the surface of airfoil determine the overall performance of an airfoil. The pressure difference on the airfoil creates lift and drag for the airfoil inducing the function of the airfoil. Typically, the shape of the airfoil have a curve leading edge and sharp trailing edge. These factors are needed on an airfoil because when fluid pass through this type of design shape it will create pressure difference between the top part and the bottom part of the symmetrical airfoil with an angle of attack directly to the flow of the fluid.

For positive angle of attack, the static pressure on top will be much lower compared to the bottom parts, this will induce the aerodynamic force exerting on the airfoil. Aerodynamic force is made from two major components the lift and drag force. Lift force is when the force is perpendicular to the direction of motion, while when the force components is parallel to

the airfoil it will create the drag force. They are many factors that affect the aerodynamic forces such as, angle of attack, shape of airfoil, density and flow speed.

When a flow surrounds an airfoil the fluid particles will start to gain velocity as it moves from the leading edge on the surface of the airfoil. This will continue until reaching the maximum velocity. This process will remain for a certain period and will start to decelerate as the particles move towards the trailing edge, this is the cause from the increasing of the static pressure. The flow will start to detach from the airfoil surface when the kinetic energy of the fluid particles is not enough to counter the increasing static pressure at the rear part of the airfoil (Sturm et al., 2012). The split of the the flow is known as the boundary layer separation. Futhermore, if the angle of attack is large the flow will be separated fully, and stall will take place. This process will then induce the reduction of lift and increase the pressure drag. Wake also will be formed behind the airfoil, the flow will take the forms of vortices.

1.3 Boundary Layer

A boundary layer is the layer that consists of fluid in the immediate vicinity of a surface, the effects of viscosity are significant in this region. The concept of boundary layer was first discovered by Prandtl (1904), he assumed that the no-slip condition at a surface where the thin layer of fluid adjacent to the surface will experience the effects of friction. As we know, the details of the flow within the boundary layer are very important. This is because these factors will induce the wing stall, skin drag friction and the heat transfer that occurs in high-speed flight. The fluid flow over an airfoil can be divided into two regions: a thin boundary layer near to the airfoil surface, in which the frictional effects are dominant and must be considered; and the region outside the boundary layer, where the friction is negligible, and the fluid is considered inviscid.

Boundary layers may be either laminar or turbulent depending on the value of Reynolds number. Laminar boundary layer is when the fluid is moving smoothly in layers, the layers slide between other adjacent layers without mixing. Disorganized and flow of random changes in pressure and velocity is the characteristics of the turbulent boundary layer. Talking about the flow separation it usually occurs at the laminar boundary layer. This is because the laminar flow has lower energy that can only handle small adverse pressure gradient. While the turbulent boundary layer, the flow will remains attached longer and separation occurs further downstream (Simpson, 2003).

1.4 Reynolds Number

Reynolds number is actually the ratio of inertial forces to viscous forces within the fluid subjected to the relative internal movement due to different fluid velocities. This parameter is indeed a dimensionless parameter. It is defined in terms of the fluid density ρ , flow velocity V , characteristic length l_c , and dynamic viscosity μ .

$$Re = \frac{\rho V l_c}{\mu} \quad (1.1)$$

Scaling factors developed with respect to laminar and turbulent flow regimes, laminar flow occurs at low Reynolds numbers ($<10^4$), where viscous forces are dominant, and is characterized by smooth, constant fluid; turbulent flow occurs at high Reynolds numbers ($>10^6$), and is dominated by inertial forces, which tend to produce chaotic eddies, vortices, and other flow instabilities.

1.5 Computational Fluid Dynamics (CFD)

Computational Fluid Dynamics (CFD) is the process use to analyse fluid flows using numerical solution methods. In spite of what preceded, with CFD it will be able to analyse complex problems involving fluid-fluid, fluid-solid or fluid-gas interaction. There are many engineering fields where CFD are frequently used such as aerodynamics and

hydrodynamics, where quantities such as lift and drag as pressures and velocities are obtained. The physical aspects of any fluid flow are governed by the following three fundamental principles: (1) mass is conserved; (2) $F = ma$ (Newton's second law); and (3) energy is conserved (Wendt et al., 2009). CFD use these aspects on the form of partial differential equations. CFD solvers transform these laws into algebraic equations and able to efficiently solve these equations numerically.

CFD analyses have a huge potential to save time in the design process and faster compared to conventional testing for data acquisition. Computational Fluid Dynamics (CFD) method are also a less costly way to study a certain problem (Gutierrez-Amo et al., 2018). A CFD solution involves a list of basic steps: (1) Pre-processing includes creation of geometry, grid generation and choice models. (2) Solving in this phase the actual computations are performed by the solver, and in this solving phase computational power is required. Application of boundary conditions and flow field computation. (3) Post processing in this phase result are visualised and analysed. Analyst can verify the result and conclusions based on the obtained data (Wendt et al., 2009).

1.6 Motivation

The behaviour of jet synthetic on the surface of leading edge of airfoil will create the existence of nonlinearities within the flow of the fluid particles. The motivation of this study is to investigate and understand the capability of jet synthetic to control the efficiency of aerodynamic properties at low-to-moderate Reynolds number. This is because in this region the flow behaviour mostly covered in the laminar flow and no major turbulent flow as turbulent flow mainly occur at high Reynolds number. This study is considered as a continuation of the effort to bring the jet synthetic full benefit, because it is proven that jet synthetic has a good potential for an active flow, even there are some problems that have not been resolved (Zhao & Zhao, 2014). In this study, ANSYS Fluent is utilized to perform the

simulations, and works is focused on NACA 4412 undergoing different jet synthetic speed and different angle of attack.

1.7 Objectives

The main objective of this study is to evaluate the effectiveness of synthetic jet in inducing leading edge vortex on the NACA 4412 airfoil. The evaluation was conducted on two parameters such as jet synthetic exit velocity (1 m/s, 2 m/s, 4 m/s, 6 m/s, 8 m/s, 10 m/s) and several angle of attacks for the airfoil (0° , 2° , 4° , 6° , 8° , 10°). This work is conducted using numerical simulation utilising Ansys Fluent software. The idea behind this work is to induce leading edge vortex in order to amplify the lift force generated by the airfoil intermittently.

1.8 Thesis Outline

There are five chapters in this thesis. CHAPTER 1 provided the introduction of jet synthetic, flow characteristics around an airfoil, Reynold's number and Computational Fluid Dynamics (CFD). Conceptual theory related to this current study and reviews on several experimental and numerical studies of other researchers are included in CHAPTER 2. In addition, theories behind the related equations and turbulence models are explained in this chapter too. CHAPTER 3 describes the computational set up of the simulation model and the validation cases performed. CHAPTER 4 shows the results obtained from the computational simulation. Also, the dynamic and unsteady aerodynamic behaviors of all cases are discussed in detail. Lastly, CHAPTER 5 concludes the works in this study and provides some suggestions for future research on similar topic.

CHAPTER 2

LITERATURE REVIEW

2.1 Flow Control

Aerodynamic flow control is the practice of controlling and manipulating a flow field through some form of actuation or interaction. This process is to ensure the change in the flow behaviour. The flow of separation and its control dominated with Prandtl when he discovered and formulated the boundary layer theory (Greenblatt et al., 2010). This process usually involves force that change the flow structure, mixing behaviour, or momentum injection in the flow field to produce more efficient performance characteristics from an aerodynamic geometry. Historically, flow control has been used to delay the laminar-turbulent transition, postpone boundary-layer separation, enhance lift, and reduce drag of an aerodynamic body, argument turbulent mixing, and suppress noise. Observations have shown that, for a certain low range of Reynolds numbers, a laminar boundary layer which separates from the surface of an aerodynamic body often reattaches to the surface subsequently as a turbulent boundary layer with a distance down the stream (Katz et al., 1998).

The fluid in these regions between the point of separation and the point of reattachment, is set into a circulatory motion (below the separated flow). The fluid in this region is generally referred as the laminar separation bubble (LSB) (Tani, 1964). Figure 2.1 shows that the schematic diagram that represents the LSB formation on an airfoil and the transition from to boundary layer to turbulent boundary layer with velocity profile at some points.

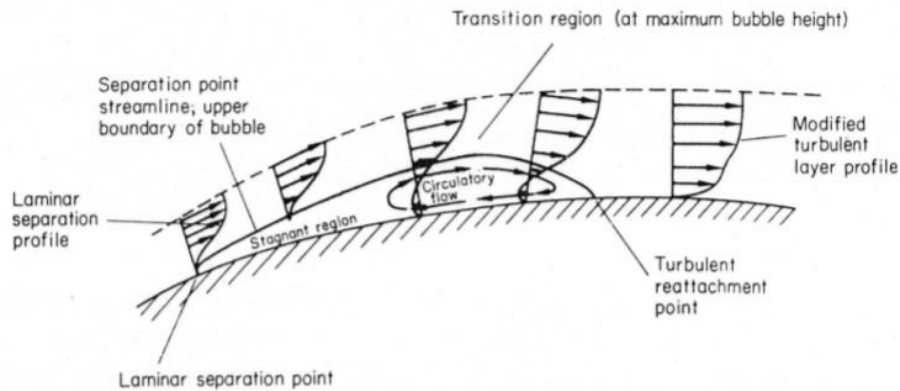


Figure 2.1: Schematic of laminar separation bubble (Crivellini et al., 2014)

The formation of LSB occurs when the small disturbances grow more readily in separated parts rather than compared to attached, boundary layers. Then, the separated laminar boundary layer will undergo transition to turbulence with characteristic thickening. This rapid thickening will then be sufficient for the lower edge of the, now-turbulent, shear layer to come back into contact and reattached in the turbulent boundary layer. The bubble of fluid will be trapped under the separated shear layer between the separation and re-attachment points (Houghton E, 2003). When the angle of incidence starts to increase to certain value, the bubble will break down. This will either cause the flow to separate completely or forming a huge and long bubble under the separated shear layer. This long bubble will have different effects on the pressure distribution action on the airfoil surface compared to the separation bubble described.

Flow around the airflow can control by introducing aerodynamic flow control. The aerodynamic flow control being introduced passively through the addition or modification of surface features, such as vortex generators vanes, serrated trailing edge geometries or dimpled surface textures. Flow also can be control actively, where actuation device is being utilized to modify and disturb the flow field. These control systems form the Active Flow Control (AFC) and Passive Flow Control (PFC).

2.2 Passive Flow Control (PFC)

The essential difference between active and passive flow control techniques is that a form of energy is needed for an active flow to control manipulate and disturb the flow. It means that, the passive flow control methods use the surrounding and does not require any exterior energy sources. A major drawback of passive flow control techniques is that it cannot be turn off and on when the situation needs, it continues to operate endlessly. Recently, most aerodynamic researchers agreed and preferred that passive flow control methods provide economically efficient and technology solutions (Serdar Genç et al., 2020a). This is because this method offers the quickest solution to be implemented and less expensive compared to the active flow control.

2.2.1 Leading Edge Slats

Slats are firstly designed as an aerodynamic surface on the leading edge of the wings of fixed-wing aircraft which, when it is deployed, allow the wing to operate at a higher angle of attack. This is the first passive control that will be discussed. This was known as a passive flow controller by delaying the flow separation, were first presented Handley in Great Britain, and was first utilized for an aircraft. The flow in space between the main body and slat created is augmented and accelerated with either large vortices or several numbers of smaller vortices as shown in Figure 2.2. Larger vortices tend to move from slat's midspan to the edge, this usually occurs at lower Reynolds number. While smaller vortices occurred at the higher Reynolds number. Which means that, flow that is accelerating with the leading-edge slats gains kinetic energy and momentum towards the boundary layer. These phenomena resulting in delaying the stall process (Rumsey & Ying, 2002). In the literature of previous research papers there are three types of slats: (1) Fixed slat (Weick & Shortal, n.d.) (2) Retractable slat (Welck & Platt, n.d.). (3) Kruger flap (Kri, n.d.). Recently, investigated on NACA2415 airfoil with NACA22 leading edge slat experimentally and

computationally. The result of the computational data concludes that LSB was correctly estimated. Thus, the process of delaying the stall phenomenon was obtained precisely by the experimental investigation. the data from the resulting in providing the maximum lift coefficient at 1.3 (Genç et al., 2009).

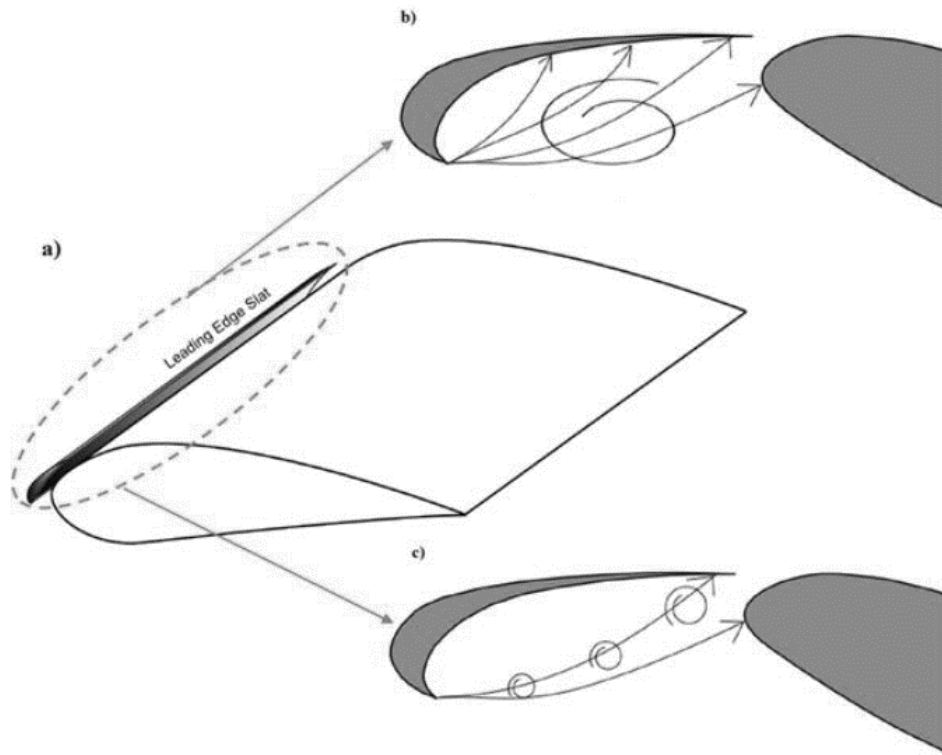


Figure 2.2: Configuration of leading-edge slat (Serdar Genç et al., 2020b).

2.2.2 Vortex Generators

A vortex generator (VG) is an aerodynamic device that consists of a small vane. This vane is usually attached to the surface of an aircraft wing or a rotor blade of a wing turbine. Vortex generators are the simplest and most efficient passive flow control devices. This device is widely used and preferred and being utilized on wind turbine blades by aerodynamic researchers. This development is to ensure that flow separation caused by Adverse Pressure Gradients (APGs) could be prohibited. Vortex generators are not only

efficient on airfoil but this device can be used in such as bluff bodies, (Aider et al., 2010), sedan cars (Masaru KOIKE, 2004), swept wings, (Langan & Samuels, 1995), and many more just to name a few. Vortex generators were first investigated by Taylor as a generally small plates having rectangular or triangular shapes on the surface of a wing (Urkiola et al., 2017). Mounted on the surface that need to flow control at angle of the incoming flow. The insertion of vortex generators usually used to decrease or even suppress the boundary layer separation, which is influenced by the APGs and turbulence effects (Schubauer & Spangenberg, 1960). When a boundary layer is moving slowly and pass through the vortex generators it energized with the conjunction of the high momentum fluid in the outer part of boundary layer and in the free stream. This process then resulting in reducing the drag force and increasing the lift force (Gao et al., 2015), (Bragg & Gregorek, 1987). Figure 2.3 shows the sketch of vortex generators on a wing.

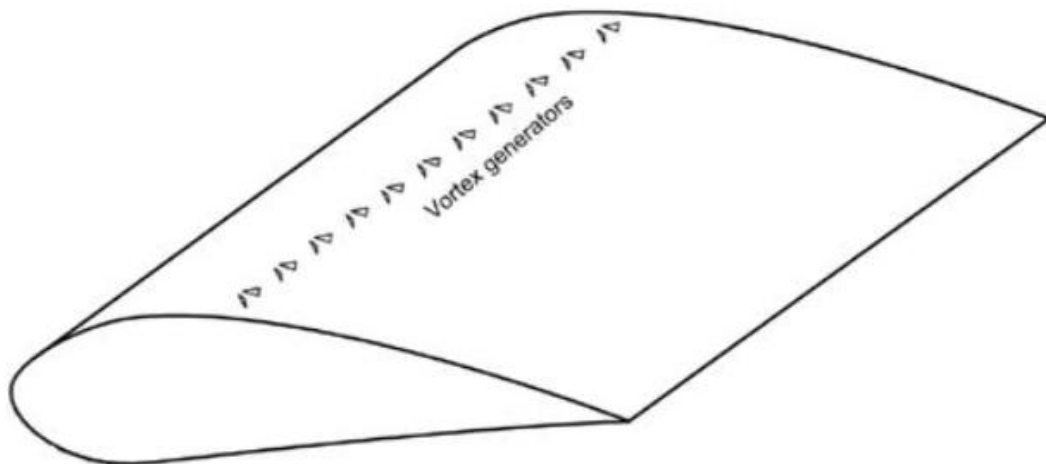


Figure 2.3: A sketch of vortex generators installed on the surface of a wing (Serdar Genç et al., 2020a).

2.2.3 Airfoils with Cavity

Trapping of vortices in a cavity has been explored in these recent years as a mechanism to reduce drag force for thick airfoils. The principle of this concept is to initiate

or create a suitable pressure gradient when there are two counter-rotating vortices are trapped inside the cavity. By having said that, these trapped vortices over the suction surface are not only for extra low-pressure region but also produce low drag. Thus, airfoils with cavity has recently gained interest among aerodynamic researchers. Investigation on airfoil with cavity at Reynolds number 2×10^4 from 0° to 15° as shown in Figure 2.4 shows delaying the stall phenomenon by means of counter-rotating separated flows, resulted in reduced flow separation region (Olsman & Colonius, 2010). A numerical study also had been done precisely regarding the aeroacoustics of NACA0018 cavitied at Reynolds number 2×10^4 and Mach number (Ma) of 0.2, the presence of the cavity on the airfoil caused the lift-to-drag ratio to increase eventually. Moreover, the cavitied airfoil produced less acoustic power, making it a noiseless and efficient airfoil design at low Reynolds number regimes (Lam & Leung, 2018).

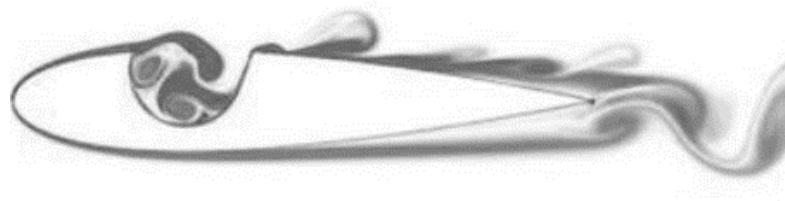


Figure 2.4: The vorticity contour plot over cavitied airfoil (Olsman & Colonius, 2010).

2.2.4 Flow Vanes

The concept of flow vanes can be utilized as a power regulator and stall controller at wing turbines, is an undiscovered item of the wind turbine blades (Pechlivanoglou, 2013). The flow vanes usually have a relatively smaller chord length compared to the main body, and this additional aerodynamic profile can be positioned over the suction surface of airfoils as shown in Figure 2.5. The gap between the flow vane and main body is closely equal to the chord length of the flow vane. In an experiment researchers found out that the cross-flow

wind turbine with a guide vane attached at the right position had a higher coefficient of power than cross flow turbine without guide vane (Santoso et al., n.d.).

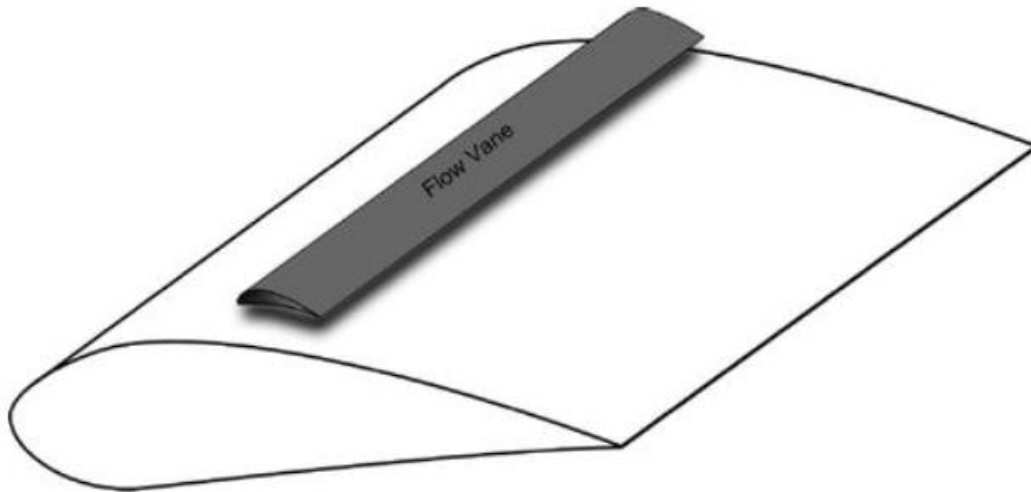


Figure 2.5: Flow vane sketch on the main body (Pechlivanoglou, 2013).

2.2.5 Roughness Material

Roughness material or surface roughness of the main body is one of the passive control methods. The objective of the roughness material is to reduce the flow separation that would occur in an airfoil at high angle of attacks. Identifying the role of roughness material on the flow characteristics over roughened NACA4412 airfoil as shown in Figure 6. The investigations to observe the force measurement, the smoke-wire, hot-film sensor, and hot wire experiments have been performed (KOCA et al., 2016). The aim of these experimental studies was to determine the LSB and transition phenomena over uncontrolled NACA4412 airfoil in detail. Moreover, to observe how sandpaper act as a roughness material affect the flow topology.



Figure 2.6: Sketch representation of the roughened airfoil at the leading edge (Serdar Genç et al., 2020a).

The result obtained from the smoke visualization experiment and hot film sensor, shows an integrated graph were shown in Figure 2.7. Streamlines of the obtained data of the smoke-wire experiment clearly show that LSB occurred between $x/c = 0.3$ and $x/c = 0.7$ for uncontrolled airfoil, while it was observed that LSB occur in the roughened airfoil. By using sandpaper causes the shrinkage of LSB's size tremendously. Physically speaking, the undulations acquired from voltage values, which were predefined started to increase after $x/c = 0.3$. The meaning of this is that the transition inception and separation point due to adverse pressure gradients in Figure 2.7(a). However, the amount of undulations at $x/c = 0.5$ was less than that at $x/c = 0.3$, because small eddies having lesser amount of energy in this region of LSB caused the undulations amount to reduce. After $x/c = 0.5$ point, the obvious increment in undulations indicated that fully turbulent flow in the boundary layer flow because of the energized vortices (Serdar GENÇ et al., 2019).

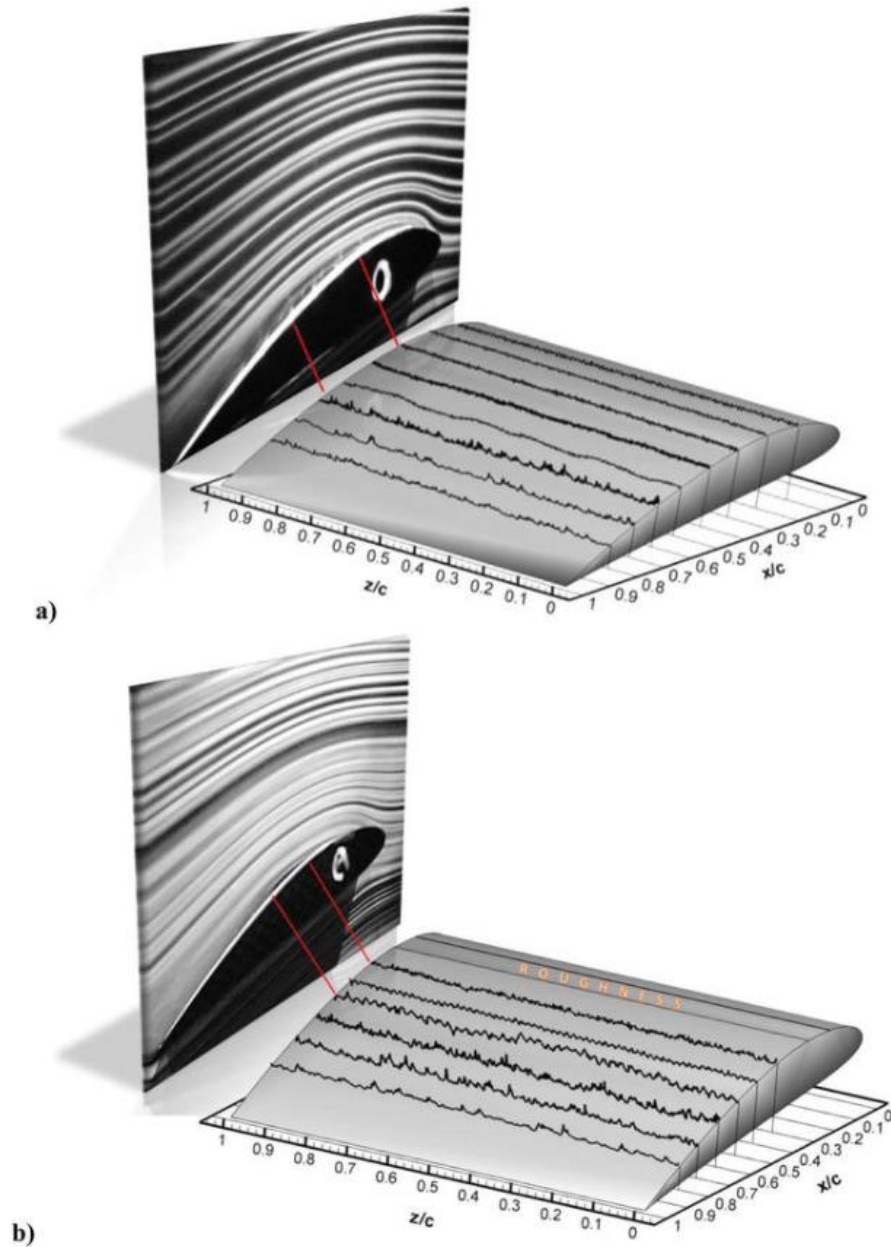


Figure 2.7: The comparison results of two different experiments at Reynolds number of 5×10^4 and $\alpha = 8^\circ$: (a) $k/c = 0$ (uncontrolled airfoil) and (b) $k/c = 0.003$ (Serdar GENÇ et al., 2019).

Figure 2.8 shows a combination of graph consisting of numerical and experimental data from the results for a roughed airfoil with $k/c = 0.006$ at Reynolds number 5×10^4 and $\alpha = 8^\circ$. At first, adverse pressure gradient (APG) exhibits a dominant role on flow, and it causes the flow separation from the surface of the airfoil at $x = 0.3$ as shown in flow

visualization graph. Moving on, the flow reattaches to the airfoil surface at $x/c = 0.6$ by gaining momentum from the roughness of the roughness material. The same flow phenomena occur, boundary layer separation, reattachment and LSB are shown and proved with streamlines and C_p curved also being obtained from the numerical experiment. The C_p curve is nearly the constant after separation point. This process is due to the presence of dead air region having as negligible as less flow phenomenon. LSB position is between $x/c = 0.3$ and $x/c = 0.6$ as shown in the smoke-wire experiment result. On the other side, a mild peak at $x/c = 0.5$ shows that the transition point over the airfoil surface.

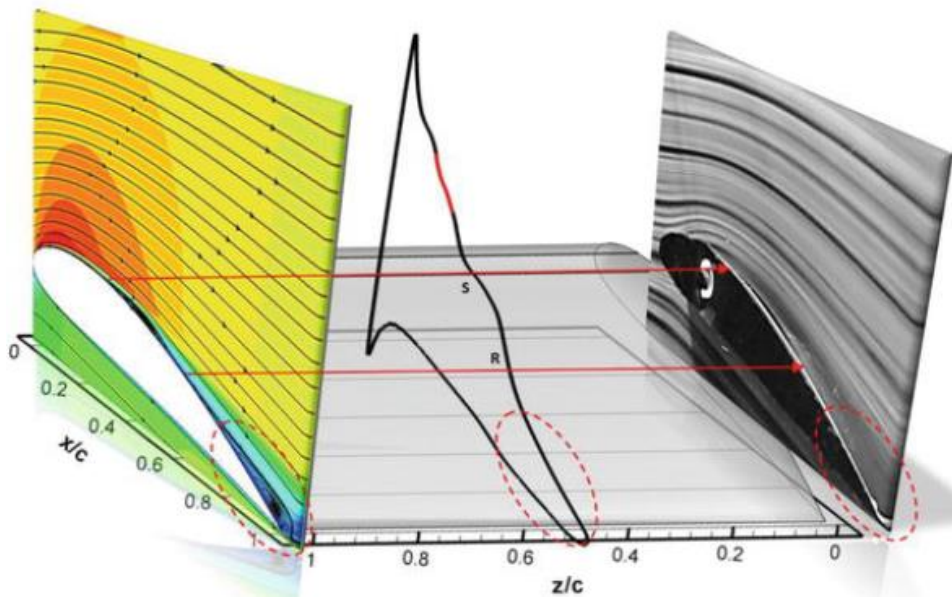


Figure 2.8: The combined result from numerical and smoke-wire result for the roughened airfoil (Serdar GENÇ et al., 2019).

Furthermore, the result mentioned above, two more important result obtained from the aerodynamic force measurement result as shown in Figure 2.9. The stall phenomenon because of flow separation was postponed if Figure 2.9 (a). Second, lift coefficient (C_L) in Figure 2.9 (b) increase with the presence of the roughness material. In spite of what preceded, the use of roughness material enhances the aerodynamic performance of the airfoil. It can be clearly seen that the roughness material also gave good result, especially in the pre-stall

region. In conclusion the roughness material was entitled as “the pre-stall flow control mechanism in aerodynamic literature by authors (Serdar GENÇ et al., 2019).

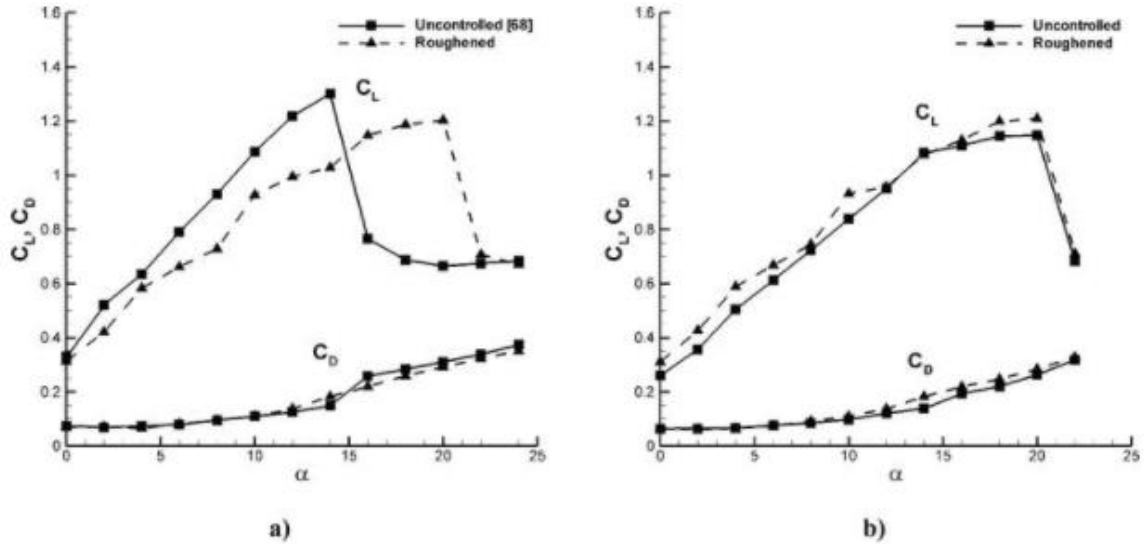


Figure 2.9: Force measurement results at $k/c = 0.006$: (a) $Re = 7.5 \times 10^4$ and (b) $Re = 1 \times 10^5$ (Serdar GENÇ et al., 2019).

2.3 Active Flow Control (AFC)

The active flow control method has two important advantages compared to the passive flow control. A passive flow control cannot be achieved with this method. The first one is to be able to control the flow with small energy outputs and to change the energy locations as needed in the body. Second, is that the turbulent region generated by complex flows can be managed and modified by the active control method. It also has the ability to operate when needed (Oktay & Kanat, 2017). The purpose of the active flow control device is the same to be able to manipulate the flow region, thus cause the decreasing of the drag in directly proportion to the decrease of the vortex and so increase the lift. There are various types of actuators used in flow control applications, and these can be classified in numerous ways. The most common type is the fluidic, which use fluid injection or suction to disturb

the flows. Next, the other class is by involving moving body. Last but not least, is the plasma actuators.

2.3.1 Fluidic Actuators

2.3.1.1 Pulsed Jet

Pulsed jet is a form of a fluidic actuators. It also has been used for many years in an open-loop applications with a great success. A pulsed jet can be generated by using, for example a fast-acting solenoid valve (Bons et al., 2002), a high-speed rotating siren valve, or the rotating orifice/slot as shown in Figure 2.10. Dc motor controls the rotational speed of the valve, and when the holes from the rotating inner body align with the fixed outer holes, air that being pressurized from the inlet is expelled. Even the bandwidth of a rotating valve may be sufficient to operate at any one of several characteristic frequencies of the flow, it is impossible to phase lock or synchronize the latter two types with a bandpass-filtered reference signal in the flow as the phase of the valve cannot be controlled.

However, if the time and frequency response of the solenoid valve are sufficient, then synchronization is possible, although the type of permissible waveforms is usually restricted to variable duty-cycle square waves. One of the main disadvantages of a pulsed jet is the required a flow source. The required average mass flow rate is usually quantified using C_μ based on the mean jet velocity and/or a dimensionless mass flow coefficient.

$$C_q = (p_j U_j A_j)/(p_\infty U_\infty A_r) \quad (2.1)$$

Where A_r is an appropriate reference area. If the mass flow rate is reduced in some manner while maintaining control authority, then the system cost of a pulsed jet may be acceptable.

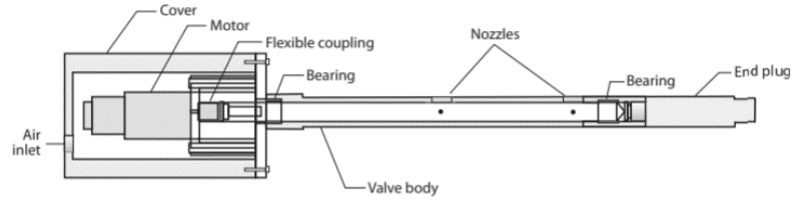


Figure 2.10: Schematic of a rotary valve (McManus & Magill, 1996).

2.3.1.2 Combustion Actuators

A combustion-driven actuator operates by using pulsed jet that are being created by ignition of mixture of gaseous fuel and oxygen in a small combustion chamber (Crittenden, 2004; Woo et al., 2011). Cycle begins as soon as injection of premixed fuel and oxidizer into the combustion chamber by replacing the remaining products from the previous cycle. A spark is required to ignites the mixture, and the combustion process usually lasts for several milliseconds. The result of the split-second combustion causes a rapid pressure to rise at the chamber being ejected to one or more high-speed jet orifices. The rate of frequency of the combustion could be adjusted to adjust the movement of the flow behaviour. Frequencies that are greater than 150 Hz can be achieved with chamber pressures of up to 5 atm, and these devices are capable of producing sonic velocities at the jet orifice. The significant jet penetration into a crossflow at Mach numbers limit up to 0.7 has been demonstrated (Crittenden et al., 2001).

The main function of this device is the ability to inject high velocity output, but due to the finite time duration and bounded with the combustion cycle, the device is limited to relatively low frequencies. Moreover, even though this device is almost similar to the other synthetic jet, this device is strictly not a zero-net-mass-flux (ZMNF). As can be seen, this device has a small but nonzero reactant flow. The rise of temperature due to the combustion process also need to be considered, this factor might affect the aerodynamic performance of the airfoil. Lastly, should be noted that the combustion actuators device is not easily to have

a feedback control mechanism due to its discrete pulse behaviour, even if the ignition could be synchronized perfectly to specific flow behaviour and conditions. Figure 2.11 shows the schematic drawing of the combustion actuators device.

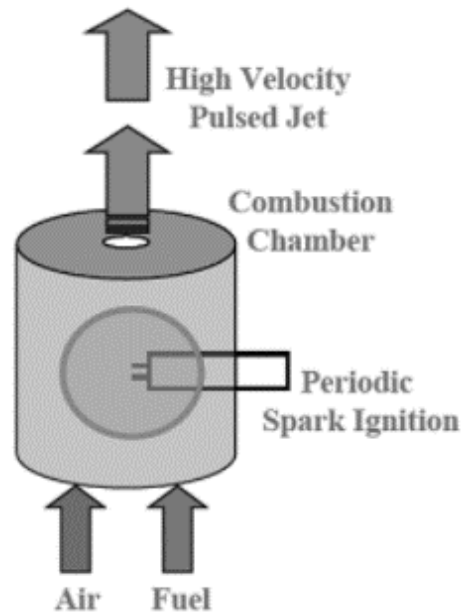


Figure 2.11: The schematic drawing of the combustion actuators device.

2.3.2 Moving Surface/Object

2.3.2.1 Piezoelectric Flap Actuators and Active Dimples

The usage of piezoelectric flap actuator has been used in various of applications, including turbulent boundary layer streaks (Jacobson & Reynolds, 1998), control of flow separation (Seifert et al., 2012), and free shear flows (Wiltse & Glezer, 1993). Normally, a cantilever composite type of beam configuration is used. The actuator can be used in spanwise or streamwise depending on the geometry and orientation of the vibrating tip with respect to the local free-stream flow (Cattafesta III & Sheplak, 2011). The beam will vibrate when an ac voltage passes through across the piezoceramic which then will interact with the flow.

A typical free-tip displacements range is from $O(10-100 \mu\text{m})$ for a device with a resonant frequency in excess of 1-2 kHz to $O(1 \text{ mm})$ when the resonant frequency reducing to a few hundred Hz or less (Kegeles et al., 2007). Discussion have been made to observe the performance trade-off inherit in the selection of microelectromechanical-syste, actuators and design, such as cantilevers (Bell et al., 2005). Figure 2.12 shows the multiple views of configuration of wind turbine blade section with active external trailing-edge flap.

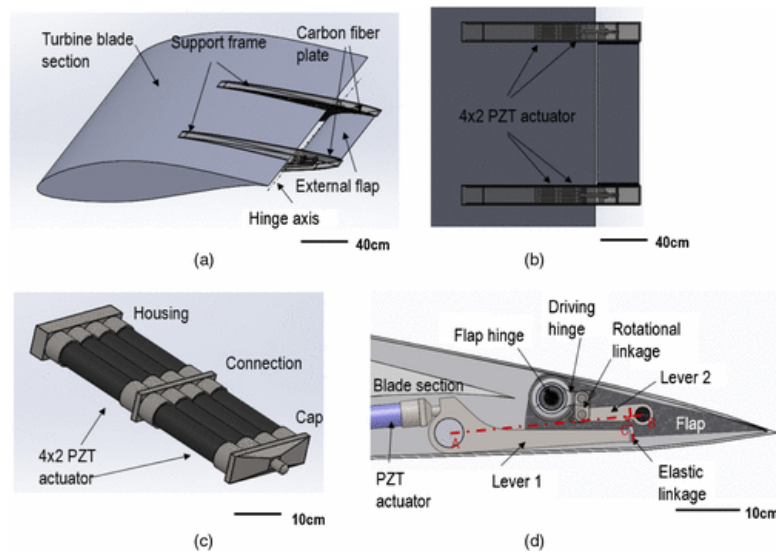


Figure 2.12: Configuration of wind turbine blade section with active external trailing-edge flap: (a) side view; (b) bottom view; (c) layout of actuator (Sun et al., 2017).

Microfabrication of electroactive polymer dimples progress has been made recently to control the flow in the turbulent boundary layers (Dearing et al., 2007). Dimple usually consists of elastomer sandwiched between compliant electrodes, when voltage flow is presence and effective mechanical is produced that is proportional to the E_{field}^2 . Nevertheless, the lateral expansion is created with the induced strain in the thickness via Poisson effect. Thus, the lateral strain is constrained at the boundary, leads to the forming of out-of-plane buckling. The dimples then created an unsteady surface depression that interact with the near-wall turbulent structures.

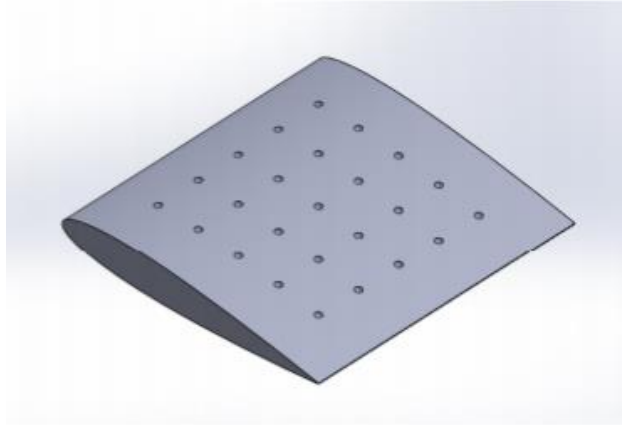


Figure 2.13: Three-dimensional view of NACA 0012 with dimples (E. Haque, n.d.)

2.4 Summary

This chapter has showed the reviews of some research on the flow control devices, both the passive and the active flow control mechanism were precisely discussed. Some of the research papers are done at low-to-moderate Reynolds number. Besides that, the works reviewed in this chapter also there are a considerably amount of numerical as well as experimental research focused on various aspects in the field of the flow control devices. The interaction between the jet synthetic mechanism and the flow around the surface of the airfoil combined together will be study further in this thesis. The physics of the fluid involved is solved by the fluid dynamics solver as in Ansys Fluent. The models of solver selected for this simulation process is the Laminar models. This is because the body of the simulation is not complex and laminar solution requires less time to be analysed. The uniqueness of the study is that possible for the insertion of normal jet synthetic without the change of mass could enhance the overall aerodynamic components and performance of the airfoil chosen.

CHAPTER 3

METHODOLOGY

3.1 Parameter Setup

The airfoil used in this study is the standard NACA 4412. There have been many studies as mentioned in CHAPTER 2, both experimental and numerical, in the behaviour of flow regarding to the jet synthetic mechanism at low-to-moderate Reynolds number employed this profile. Some examples of works have been reviewed about the jet synthetic in CHAPTER 1 and 2, for instance the numerical studies by (Kim et al., 2019), and the experimental works done by (Gardner et al., 2014). The published data from these researchers can be used as a method of validation and comparison purpose.

Table 3.1 below listed all the physical and geometric properties used in the process of modelling the jet synthetic mechanism in the leading edge of the airfoil. These values are partially acquired from the research paper mentioned earlier, the properties of the airfoil were determined by multiple numerical study to select the best parameters that enhance the aerodynamic properties of the airfoil. The velocity of the inlet in the simulation is also pre-determined. There are some of the properties of the airfoil and air that is being considered.

Table 3.1: Properties of air and airfoil.

Parameter	Value	Unit
Density of air, ρ	1.225	kg/m^3
Density of airfoil, ρ	2719	kg/m^3
Viscosity of air, η	1.789×10^{-5}	kg/ms^{-1}
Chord length, c	1.0	m

In this study, five cases with different velocity of the jet are tested. The velocities of jet are inserted by the transient table features on the ANSYS Fluent. The magnitude of the jet velocities selected to be tested are 1 m/s, 2 m/s, 4 m/s, 6 m/s, 8 m/s, 10 m/s. The jet velocities are also set to be flow out at 5 s, 7 s, and 9 s out of the 10 s simulation process. The distance of orifice for the jet is also determined, the distance is from $0.1 c$ to $0.12336 c$. By subtracting the initial and final point of the orifice, the distance of the hole is 0.02336 m.

3.2 Fluid Solver

The chosen fluid solver for this current study is the commercial CFD code Ansys Fluent 2019 R3. First and foremost, the simulation model and domain are modelled by importing the NACA 4412 airfoil profile into ANSYS DesignModeler and creating surfaces with the lines imported. Then, the modelled domain is meshed using the ANSYS Meshing, in which the domain will be divided into numerous small elements. The mesh file is then updated and imported into the fluid solver ANSYS Fluent to set up the simulation and calculate the solution for the numerical problem.

3.2.1 Mesh and Boundary Conditions

For the meshing process, the unstructured grids are used for the flow domain with structured inflation layers around the surface of the airfoil. Figure 3.1 shows the mesh produce around the airfoil. The number of inflation layers applied is 15 and the maximum thickness of the inflation is set at 0.005 m to ensure the Y-plus of the simulation data is accurate and close to one. The Y^+ value is a non-dimensional distance from the wall to the first mesh node on the local cell fluid velocity. If the Y-plus value is too large and not nearly to one, this will be resulting in the calculations of pressure and velocity near the surface of the airfoil is inaccurate.